CrossMark

ORIGINAL PAPER

Spherical nanocomposite particles prepared from mixed cellulose–chitosan solutions

Jiayi Yang · Jiangjiang Duan ·
Lina Zhang · Björn Lindman ·
Håkan Edlund · Magnus Norgren

Abstract Novel cellulose–chitosan nanocomposite particles with spherical shape were successfully prepared via mixing of aqueous biopolymer solutions in three different ways. Macroparticles with diameters in the millimeter range were produced by dripping cellulose dissolved in cold LiOH/urea into acidic chitosan solutions, inducing instant co-regeneration of the biopolymers. Two types of microspheres, chemically crosslinked and non-crosslinked, were prepared by first mixing cellulose and chitosan solutions obtained from freeze thawing in LiOH/KOH/urea. Thereafter epichlorohydrin was applied as crosslinking agent for one of the samples, followed by water-in-oil (W/O) emulsification, heat induced sol–gel transition, solvent exchange, washing and freeze-drying. Characterization by X-ray photoelectron spectroscopy, total elemental analysis, and Fourier transform infrared spectroscopy confirmed the prepared particles as being true cellulose–chitosan nanocomposites with different distribution of chitosan from the surface to the core of the particles depending on the preparation method. Field emission scanning electron microscopy and laser diffraction was performed to study the morphology and size distribution of the prepared particles. The morphology was found to vary due to different preparation routes, revealing a core shell structure for macroparticles prepared by dripping, and homogenous nanoporous structure for the microspheres. The non-crosslinked microparticles exhibited a somewhat denser structure than the crosslinked ones, which indicated that crosslinking restricts packing of the chains before and under regeneration. From the obtained volume-weighted size distributions it was found that the crosslinked microspheres had the highest median diameter. The results demonstrate that not only the mixing ratio and distribution of the two biopolymers, but also the morphology and nanocomposite particle diameters are tunable by choosing between the different routes of preparation.

Keywords Cellulose · Chitosan · Nanocomposite · Microspheres · Regeneration

J. Yang · B. Lindman · H. Edlund · M. Norgren (✉)
FSCN, Surface and Colloid Engineering, Mid Sweden University, 85170 Sundsvall, Sweden
e-mail: magnus.norgren@miun.se

J. Duan · L. Zhang
College of Chemistry and Molecular Sciences, Wuhan University, Wuhan 430072, China

Introduction

The need for society to replace oil-based based fuels and materials with products derived from renewable resources is growing along with reports on increasing carbon dioxide content in the atmosphere, causing climate change. Among the most abundant renewable biomaterials, suitable for this purpose, are cellulose

from wood and chitosan derived by degradation of chitin from the exoskeleton of crustaceans. Utilization of cellulose and chitosan in different composite materials has been studied for decades (Nishio 1994; Peter 1995). Both biopolymers have β-glucosidic bonds and very similar structure. Their somewhat unique properties; especially the strong mechanical strength, biocompatibility and thermal stability of cellulose (Nishio 1994; Yamashiki et al. 1990), and the wound healing, antibacterial properties of chitosan (Burkatovskaya et al. 2006; Jain and Banerjee 2008; Kiyozumi et al. 2006; Shepherd et al. 1997), as well as their ability of self-assembly into intriguing micro- or nano-sized structures (Qiu and Hu 2013; Wu et al. 2016; Zhang et al. 2016), provide many options and ideas for functional materials design.

In preparing novel cellulose–chitosan biocomposites, we need usually to disassemble the molecular networks, either directly or after chemical modification (Chundawat et al. 2011) and to mix the two polymers. Among the different ways of disassembly, dissolution enables to separate the polymer chains from each other and produce molecular "bricks" for construction of novel materials (Trygg 2015). For a given semicrystalline polymer, such as cellulose, the chains are more in the regular, arrangement and it is rather difficult to unfold the well-packed chains into a disordered state in solution (Lindman et al. 2010; Medronho and Lindman 2014). Over decades the hydrogen bonds network in cellulose has been claimed as the reason of the crystalline structure of cellulose and the limitations in cellulose dissolution (Bodvik et al. 2010; Zhang et al. 2002), while the amphiphilic nature of cellulose has probably been underestimated (Medronho et al. 2012, 2015). Thus, when developing efficient solvents for cellulose dissolution, not only the intermolecular hydrogen bonds need to be overcome, but also the hydrophobic chain interactions have to be minimized (Glasser et al. 2012; Medronho et al. 2012).

The history of dissolving cellulose can be dated back to 150 years ago when the first time chemically modified cellulose dissolution was introduced (Liebert 2010). Since then the ideas of dissolving derivatized cellulose became widespread and it is still dominating in the industry. Today, commercial production is either carried out via the viscose (Huber et al. 2011; Klemm et al. 2004) or the Lyocell processes (Rosenau et al. 2002), using derivatizing and non-derivatizing

solvents, respectively; these processes involve toxic derivatization steps or toxic and expensive chemicals. There are other known routes for cellulose dissolution with inorganic complexes (Miyamoto et al. 1995; Saalwächter et al. 2000), or certain exotic organic solvents (Philipp 1993), which, however, cannot be considered sustainable for large scale production. In the early 1990s, alkali-based aqueous solvents started to gain more academic and technical attention for the reasons of being more environmental benign than other protocols (Isogai and Atalla 1998; Kamide et al. 1992; Zhou and Zhang 2000). Especially the later research on cold sodium hydroxide-urea or thiourea solutions broke the threshold of dissolving cellulose of higher molecular weights (Cai et al. 2008; Zhang et al. 2002; Zhou and Zhang 2000). Cellulose can also be dissolved in phosphorous acid and some other strong acids, but usually depolymerization of the cellulose chains takes place markedly more rapidly than in alkaline solutions (Hao et al. 2015; Medronho and Lindman 2014). In contrast to cellulose, chitosan is dissolved already under weakly acidic conditions due to protonation of amine groups in the structure (Pillai et al. 2009). Studies of dissolving chitin and chitosan in aqueous alkaline solvents have been carried out recently, for preparing different functional materials (Duan et al. 2015a, b; Fang et al. 2015). With the success of dissolving chitosan in cold alkali/urea solvents, opportunities to study mixed cellulose–chitosan solutions are emerging. Based on mixed solutions, a tunable homogeneous cellulose–chitosan nanocomposite could be envisaged and this could grant the material with interesting characteristics derived from the most significant properties of the individual biopolymers; strength of cellulose and bioactivity of chitosan.

In the present work, three different types of cellulose–chitosan nanocomposites, in the form of spherical particles of different sizes, were prepared. Cellulose and chitosan were dissolved in LiOH/urea and LiOH/KOH/urea solvents, respectively, via a freezing-thawing process (Duan et al. 2015b). Cellulose–chitosan particles (CCP) were obtained by dripping cellulose solution into a solution of chitosan in a dilute acetic acid. Cellulose–chitosan microspheres, with and without the addition of crosslinking agent (CCMS-CL and CCMS, respectively), were prepared via sol–gel transition in water-in-oil (W/O) emulsions.

Materials and methods

Materials and chemicals

The cellulose used was a commercial sulfite dissolving pulp provided by Domsjö Fabriker Aditya Birla (Örnsköldsvik, Sweden), with viscosity of 450 mL g^{-1}. Commercial grade chitosan from shrimp shells was supplied by Regal Biology Ltd. (China), and the degree of deacetylation was determined to 89 % by potentiometric titration (Duan et al. 2015b). The other chemicals; lithium hydroxide (LiOH), potassium hydroxide (KOH), urea, acetic acid, epichlorohydrin, t-BuOH, isooctane and Span®80, were of analytical grade and supplied by Shanghai SHENSHI Chemical Co, Ltd (Shanghai, China).
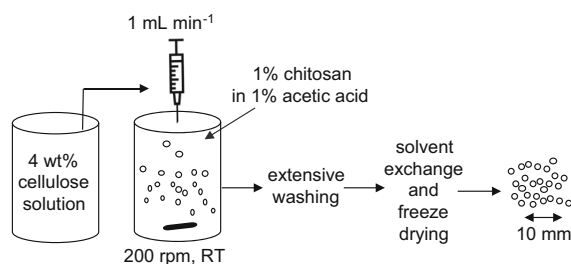
Dissolution of cellulose and chitosan

Cellulose and chitosan dissolution was achieved in different aqueous solvents. For cellulose, an aqueous solvent containing LiOH/urea/water (4.6:15:80.4 w/w) was prepared and frozen for dissolving purpose. 4 g of cellulose was dispersed with extensive stirring in 96 g of thawed LiOH/urea solvent. The mixture was then kept at −35 °C until it was completely frozen, and then thawed at room temperature and stirred at 1300 rpm for 2 min to dissolve cellulose. This freezing/thawing/stirring circle was repeated two more times until cellulose was fully dissolved. A 4 wt% transparent cellulose solution was obtained after removing the air bubbles by centrifuging the sample at 8000 rpm and 0 °C for 10 min. Chitosan solutions were prepared in two manners; conventional dissolution in 1 % acetic acid and dissolution in LiOH/KOH/urea (Duan et al. 2015b). The 1 wt% solution of chitosan in acetic acid was prepared by mixing the required amount of chitosan in 1 % acetic acid at room temperature. For the latter chitosan solution, 4 g of chitosan was dispersed in 96 g of LiOH/KOH/urea/water solvent (4.6:7:8:80.4 w/w) with stirring at 1300 rpm for 5 min. Then the mixture was stored at −35 °C until it was totally frozen. The frozen mixture was then fully thawed and stirred at 1300 rpm for 2 min. The sample went through two more freezing/thawing/stirring circles to get chitosan fully dissolved. Then the mixture was degasified by centrifugation at 8000 rpm and 0 °C for 10 min to obtain a transparent chitosan solution.

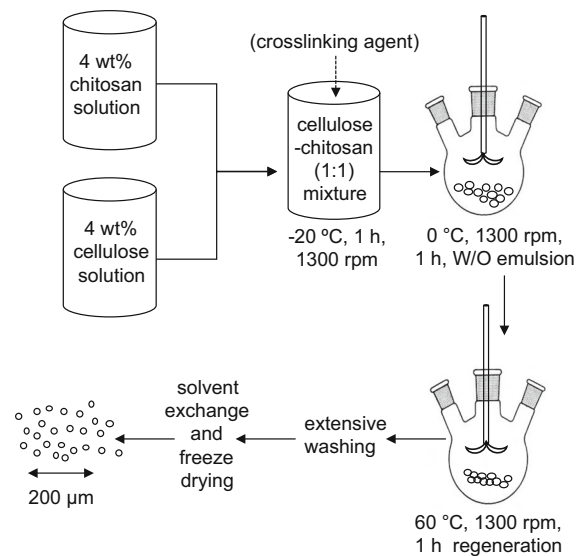### Preparation of cellulose–chitosan nanocomposites

Particles with different sizes, from a few millimeters to diameters ranging from 5 μm to over 100 μm, were prepared via the different procedures described below. For cellulose–chitosan macroparticles (CCP), showed in Scheme 1, 10 mL cellulose solution was added to 100 mL of 1 wt% chitosan at a rate of 1 mL min^{-1} by using a syringe pump. During the addition, the bulk solution was agitated with a magnetic bar at 200 rpm. The regenerated particles were then collected and washed extensively in deionized water to remove salts, followed by solvent exchange from water to t-BuOH before freeze-drying.

Crosslinked cellulose–chitosan microspheres (CCMS-CL) and cellulose–chitosan microspheres without crosslinking (CCMS), were prepared as shown in Scheme 2. Equal amounts of 4 wt% cellulose solution and 4 wt% chitosan solution were mixed at −20 °C for 2 h at 1300 rpm. At the given mixing ratio the cellulose–chitosan solution did not show any signs of phase separation. To induce crosslinking between cellulose and chitosan, epichlorohydrin was added to the mixture (Chang et al. 2010; Duan et al. 2015b). Meanwhile, an oil phase was prepared by mixing isooctane and Span® 80 (100:1 v/v) at 1300 rpm for 30 min at room temperature in a three-neck round-bottom flask. The ready blend of crosslinked cellulose–chitosan was immediately added into the oil phase under gentle agitation. Hereafter the water-in-oil (W/O) emulsion was agitated at 1300 rpm and 0 °C for 1 h to obtain stable cellulose–chitosan biocomposite spheres. Subsequently, the emulsion was heated to 60 °C for 1 h in a water bath to induce sol–gel transition by worsening the solution conditions

Scheme 1 Preparation of regenerated cellulose–chitosan macroparticles (CCP) by dripping cellulose solution into acidic chitosan solution. 4 wt% cellulose in LiOH/urea/water (4.6:15:80.4 w/w) is prepared via freezing/thawing procedure, and t-BuOH is used for solvent exchange

Scheme 2 Preparation of cellulose–chitosan microspheres, crosslinked with epichlorohydrin (CCMS-CL) and non-cross-linked (CCMS), in water-in-oil emulsion. 4 wt% cellulose in LiOH/urea/water (4.6:15:80.4 w/w) and 4 wt% chitosan in LiOH/KOH/urea/water (4.6:7:8:80.4 w/w) are prepared via freezing/thawing procedure, and t-BuOH is used for solvent exchange

for the polymers (Duan et al. 2015a; Medronho and Lindman 2015). The resulting suspension containing cellulose–chitosan microspheres was then washed extensively in ethanol/water (6:4 v/v) to remove residual isooctane and Span® 80, and thereafter continually washed in deionized water to remove salts. Finally, the spheres were subjected to a solvent exchange with t-BuOH before freeze-drying.

Chemical and physical characterization

X-ray photoelectron spectroscopy (XPS) was performed on a Thermo Fisher ESCALAB 250Xi spectrometer, equipped with Al Kα radiation as the monochromatic source. The surface compositions of carbon, oxygen and nitrogen were recorded for the three different nanocomposites. To obtain the total composition of the prepared material, elemental analysis of carbon, oxygen, hydrogen and nitrogen was conducted on a Flash 2000 organic element analyzer according to an accredited method at DB lab (Copenhagen, Denmark), using duplicate analysis. In order to further verify the composition of the cellulose–chitosan nanocomposites, Fourier transform infrared spectroscopy (FTIR) was conducted over a

wavelength range of 400–4000 cm^{-1} on a Nicolet Magna 750 spectrometer to check the existence of amino groups from chitosan. X-ray diffraction (XRD) was carried out to observe the diffractive patterns in raw material and the prepared nanocomposites. The experiments were conducted on a Bruker D2 phaser XRD diffractometer, with Cu Kα radiation of 1.54 Å at 30 kV and 10 mA, and recorded in the region of 2θ from 10° to 45° at a scanning rate of 0.01 °s^{-1}. The appearance, surface structure and morphology of the nanocomposite particles were investigated with a field emission scanning electron microscope (SEM) from Zeiss Merlin. The samples were coated with gold/platinum and the secondary electron images were generated using 5 kV accelerating voltage and an in-lens detector. Volume-weighted size distributions of the microspheres were determined by laser diffraction on a Malvern Mastersizer 2000, using a He–Ne gas laser red light with a beam wavelength of 633 nm and a LED blue light with a wavelength of 466 nm. The samples in deionized water were dispersed in an ultrasound water bath at 80 W for 2 min before the size distributions were recorded.

Results and discussion

Chemical characterization by XPS, elemental analysis and FT-IR

In the present work, two completely different routes were applied in the preparation of the nanocomposite particles; dripping of cellulose solution into an acidic regeneration bath containing chitosan or mixing of alkaline cellulose and chitosan solutions, followed by emulsification and temperature induced sol–gel transition to regenerate the nanocomposite spheres. Thus, the molecular interactions between cellulose and chitosan and thereby the distribution of the two polymers in the particles were assumed to be different and of importance to investigate. Firstly, the surface chemistry of the three samples were investigated with X-ray photoelectron spectroscopy (XPS). As seen in the XPS spectrum of all three samples presented in Fig. 1, there is a strong peak at 399.3 eV that corresponds to the binding energy of N$_{1S}$ (Wang et al. 2016; Xiang et al. 2011). The nitrogen signal, only arising from the amino groups of chitosan, reveals the presence of chitosan in the surface layer of
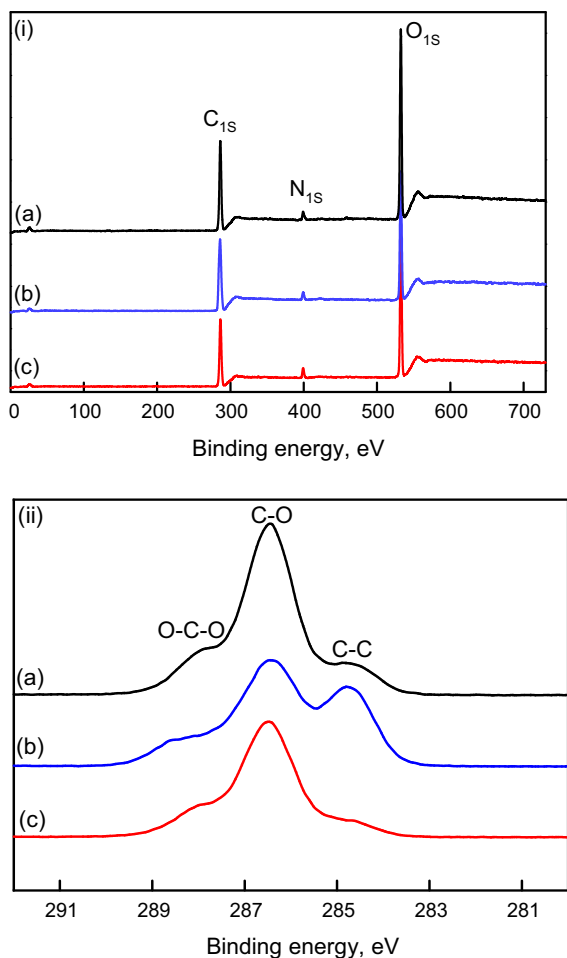
Fig. 1 **i** XPS spectra of different cellulose–chitosan particles showing C_{1S}, N_{1S} and O_{1S} binding energies, **ii** XPS spectra with magnified C_{1S}. (*a*) macroparticles, CCP; (*b*) chemically cross-linked microspheres, CCMS-CL; (*c*) non-crosslinked microspheres, CCMS

the biocomposites and indicates that chitosan molecules really are interlocked, making the materials into true nanocomposites. The C_{1S} peak is divided into three parts, at 287.8, 286.4 and 284.9 eV. The peaks indicate the O–C–O, C–OH and C–C bonds (Belgacem et al. 1995), respectively; these exist in both cellulose and chitosan. A third peak appears at 532.8 eV and corresponds to the O_{1S} assigned to the hydroxyl groups.

To further investigate any differences in biopolymer interaction due to the different preparation methods, the overall nitrogen content was determined by elemental analysis. The surface elemental compositions from the XPS analysis and the overall

elemental compositions are listed in Table 1. The CCP sample, prepared by the dripping method, shows a nitrogen content of 2.96 % in the surface layer. However, the elemental analysis of the CCP sample reveals a significantly lower total nitrogen content. The difference is obviously due to the preparation procedure. When cellulose is dripped into the acidic chitosan solution, the polymers are rapidly mixed at the interface of the droplet, but the instant pH change promotes instability of cellulose. Since the co-regeneration starts on the outermost surface of the cellulose droplets, polymer chain entanglements with chitosan are formed under the solidification phase. This slows down further diffusion of chitosan from surface to the core of the particles. Thus chitosan is enriched at the surface, as shown by the higher nitrogen content on the surface of CCP in comparison to the overall nitrogen content.

As can be seen in Table 1, the CCMS-CL and CCMS nanocomposites prepared from alkaline solution mixing, emulsification and temperature induced sol–gel transition, show higher nitrogen content than CCP, both in the surface layer and overall. The nitrogen content in a fully deacetylated chitosan molecule is about 8.7 % (hydrogen not included in total mass calculation), and in the homogeneously mixed cellulose–chitosan spheres prepared in this study about half of that nitrogen content is expected. The latter was also determined, as shown in Table 1. A similar nitrogen content from surface to bulk implies that the chitosan and cellulose were well-dispersed in the mixed solution and stability was maintained during the emulsification and solidification. The difference in nitrogen content between the surface layer and the bulk in the composite materials also indicates that it is possible to tune the chitosan distribution via choice of preparation method.

The very similar nitrogen content in crosslinked CCMS-CL and non-crosslinked CCMS further indicates that co-regeneration of cellulose and chitosan gives rise to equally stable nanocomposites as in CCMS-CL, where cellulose and chitosan were cross-linked before solidification. The strong mixing of cellulose and chitosan via chain entanglements prevented detachment of chitosan, even though the nanocomposites were extensively washed with water in the preparation procedure. The small difference in nitrogen content still detected, was probably due to the addition of crosslinking agent in CCMS-CL, which

Table 1 Surface composition from XPS and overall composition from elemental analysis of CCP, CCMS-CL and CCMS

Element	XPS (%)			Elemental analysis (%)		
	CCP	CCMS-CL	CCM	CCP	CCMS-CL	CCM
Carbon	56.2	64.0	56.2	47.4	47.1	46.9
Oxygen	40.9	32.8	39.6	51.7	49.0	49.1
Nitrogen	2.96	3.21	4.24	0.97	3.92	4.04

introduced extra carbons to the composite, making the carbon content and total accounted mass slightly higher.

Compared to the theoretical carbon/oxygen ratio in cellulose $(C_6O_5H_{10})_m$ and chitosan $(C_6O_4H_{11}N)_n$, the XPS analysis showed higher carbon and lower oxygen content, while the outcome of the elemental analysis showed a carbon/oxygen ratio close to the theoretical value. This is most likely due to surface contamination, leading to an overestimation of carbon in the XPS analysis (Edgar and Gray 2003). The difference in carbon/oxygen ratio between CCMS-CL and CCMS is probably due to the presence of crosslinks in CCMS-CL, which increases the carbon/oxygen ratio.

FTIR offers a fast and straightforward analysis of functional groups that might provide complementary information on the composition in composite materials. Figure 2 shows the FTIR spectra of cellulose, chitosan and the three prepared nanocomposites. Within the 1800–400 cm^{-1} spectral window, the characteristic absorption bands of chitosan are situated at 1646 and 1570 cm^{-1}, corresponding to the C=O stretching from amide I and the –NH bending from amide II, respectively, similar to what is found in the literature (Cao et al. 2016; Cheng et al. 2003; Duan et al. 2015a). In the spectrum of cellulose, a characteristic band due to –OH is found at 1641 cm^{-1} (Kingkaew et al. 2014). For all three prepared samples there are characteristic amide bands from chitosan, slightly shifted to 1652 cm^{-1} respective 1592 cm^{-1} because of the interactions between cellulose and chitosan functional groups (Bof et al. 2015). This is attributed to similar chemical and geometrical structures of cellulose and chitosan, also affecting the compatibility of the two polymers in the nanocomposites.
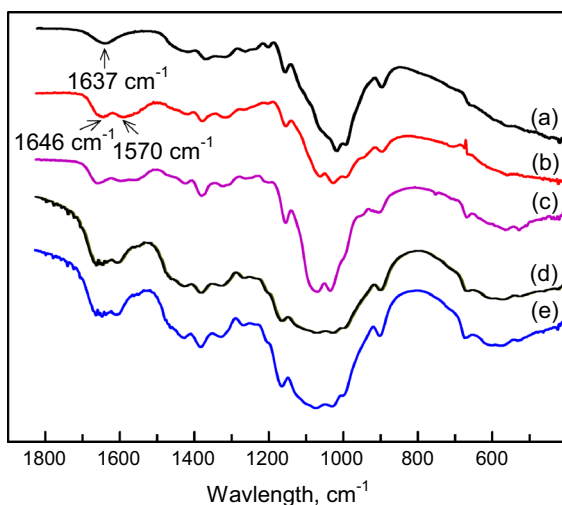
Analysis of particle morphology by FE-SEM

The different preparation methods, and the differences in chitosan distribution between the three composite particles, made it interesting to investigate the morphology of the prepared particles. The images in Fig. 3 obtained by FE-SEM analysis qualitatively show the sizes and the surface morphologies of the particles in the samples. As shown in Fig. 3a-1, a-2, the particles in the CCP sample were not in a perfect spherical shape probably due to deformations induced during agitation of the sample after the dripping. The sizes of the particles were in the range of about 1–3 mm. As is revealed in Fig. 3a-3, a-4 showing a partly broken particle, the CCP particles were found to exhibit a "shell" structure, and the outermost layer shows a morphology different from the interior of the particle, that displays a typical polymer chain network. This observation in correlation with the XPS and the analysis of the nitrogen content in this sample
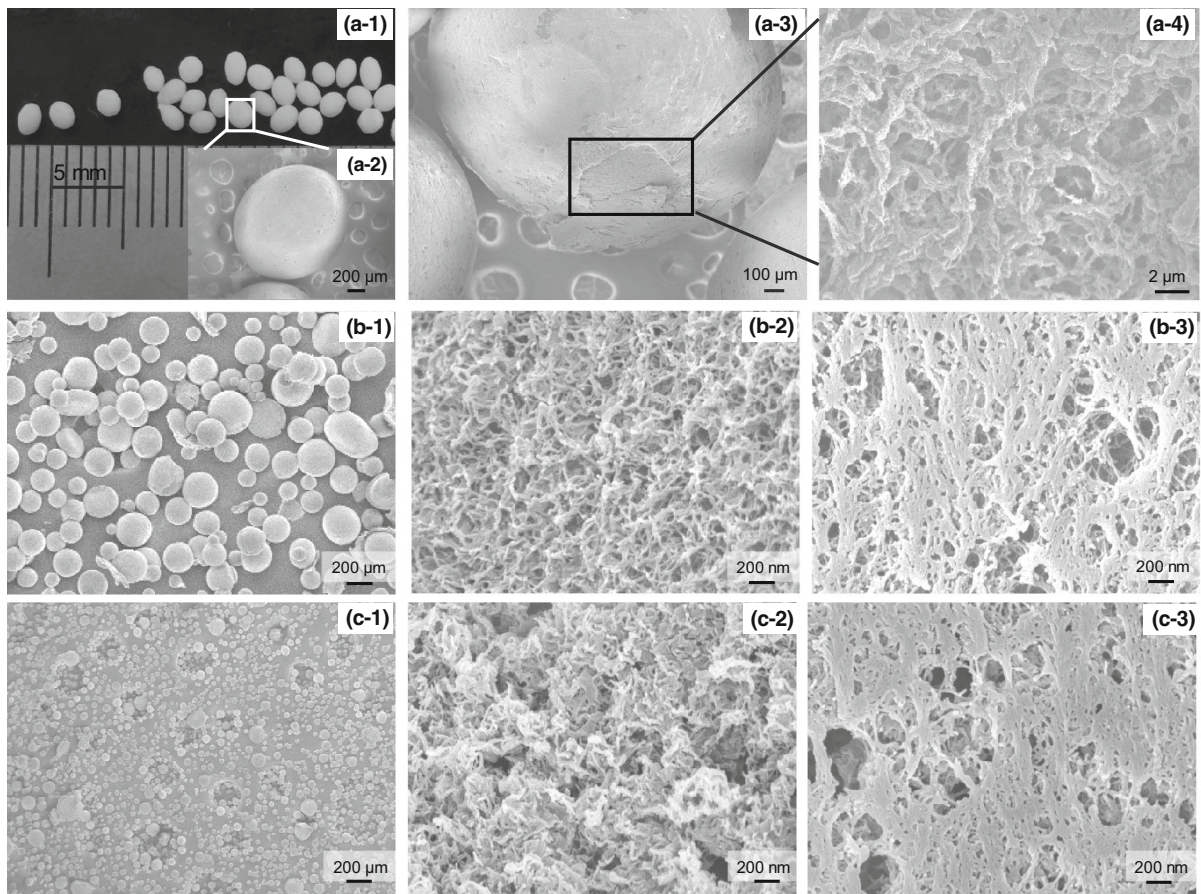

Fig. 2 FT-IR spectra of (*a*) cellulose; (*b*) chitosan; (*c*) macroparticles, CCP; (*d*) chemically crosslinked microspheres, CCMS-CL and (*e*) non-crosslinked microspheres, CCMS

Fig. 3 FE-SEM images at different magnification of the biocomposite particles prepared with different routes, **a** macroparticles, CCP; **b** chemically crosslinked microspheres, CCMS-CL and **c** non-crosslinked microspheres, CCMS

indicates that the shells are enriched in regenerated chitosan. Compared with CCP, the CCMS-CL and CCMS biocomposite particles show perfect spherical shapes. In Fig. 3b-1, c-1, it is clear that the CCMS-CL and CCMS particles have different average sizes, where CCMS-CL with the addition of crosslinking agent before emulsification gives larger particles.

When comparing the surface morphology of the microspheres prepared by emulsification of polymer mixtures (Fig. 3b-2, c-2), CCMS-CL and CCMS also show different nano-structures. CCMS-CL displays a fine porous network of the regenerated polymer chains, while for the CCMS microspheres the structure is more condensed. Probably the crosslinking agent decreases the degree of freedom of cellulose and chitosan molecules and restricts the polymer chain packing in the emulsion droplets, and thereby partially locks the structure already before the sol–gel transition

takes place. Thus, the applied crosslinking agent does not only affect the size distribution of the particles, but also the morphology in terms of the nano-structure of the microspheres. Accordingly, the same features can be noticed from the cross sections of the microspheres displayed in Fig. 3b-3, c-3, showing a larger amount of fine pores in CCMS-CL than in CCMS. The additional relatively large pores found both in CCMS-CL and CCMS were probably artifacts derived from freezing and sublimation of t-BuOH during freeze drying.

Analysis of nanocomposites by XRD

In Fig. 4, the results from XRD analysis on raw materials and prepared nanocomposites can be viewed. The pure cellulose sample shows a typical cellulose I structure, with diffraction peaks at 15.5°,
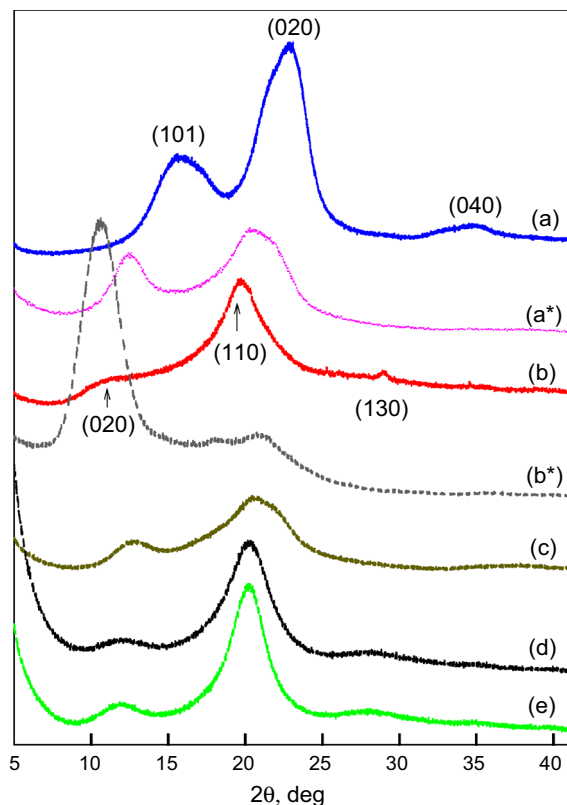
Fig. 4 The XRD patterns of raw materials and the three nanocomposite samples; (*a*) cellulose, (*a**) regenerated cellulose, (*b*) chitosan, (*b**) regenerated chitosan, (*c*) macroparticles, CCP, (*d*) chemically crosslinked microspheres, CCMS-CL, and (*e*) non-crosslinked microspheres, CCMS

22.8° and 34.5°, assigned to (101), (002) and (040), respectively. The major peak at 22.8° (002) is typical for cellulose I crystalline polymorph (Hasegawa et al. 1992; Nishino et al. 1995). After regeneration, the characteristic diffraction peak of cellulose II was detected at 20.7° (Freire et al. 2011). The pure chitosan raw material shows diffraction peaks at 11.9°, 19.7° and 29.1° that can be assigned to (020), (110) and (130), respectively (Zhang et al. 2005). The diffraction peaks at 11.9° (020) and 19.7° (110) represent the amorphous and the crystalline regions of chitosan (Yang et al. 2012). The regenerated chitosan, showing a strong peak at 10.6° and a minor peak at 20.7°, has a diffraction profile, which is rather different than the raw material. This implies a dominant amorphous feature of the regenerated chitosan (Yang et al. 2012). If the compatibility between cellulose and chitosan would have been poor in the nanocomposite materials, their diffraction peaks would have been found at the

same positions as in the individual, regenerated raw materials. Comparing the raw materials with the nanocomposites, there were only two diffraction peaks detected at 12.2° and 20.1° in the three prepared samples. The new diffraction profiles indicate that cellulose and chitosan show excellent compatibility in the nanocomposites, otherwise there would have been diffraction peaks from cellulose or chitosan (Cao et al. 2016). Moreover, the shifting of the diffraction peaks implies that there are new arrangements of the polymer molecules in the biocomposites. Both cellulose and chitosan suffer structure changes during the co-regeneration, and the development of new hydrogen bond networks have probably contributed to the new diffraction profiles.

Size distribution of the microparticles

As seen in Fig. 3, the CCMS-CL and CCMS microspheres seem to exhibit significant differences in size. From microscopy it is however only possible to determine size distributions locally and many images have to be analyzed to get sufficient statistical significance. Therefore, 4 wt% CCMS-CL and CCMS were dispersed in water and the size distributions were analyzed by laser diffraction. In Fig. 5, the size distributions of the spheres can be viewed. The CCMS sample shows a volume-weighted median diameter of 30.2 μm. The sample contains a small fraction with diameters around 1000 μm, which is most likely due
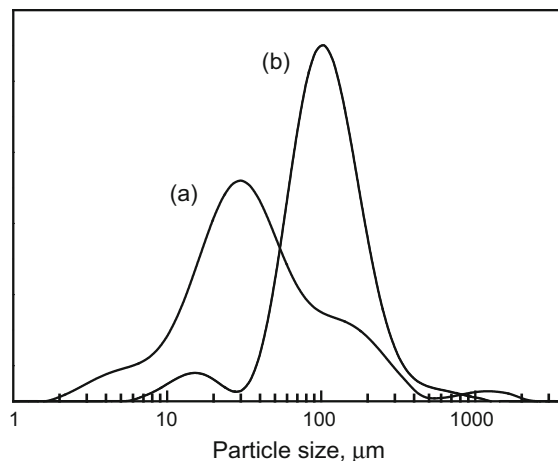

Fig. 5 Volume-weighted size distributions of the prepared cellulose–chitosan microspheres obtained by laser diffraction; (*a*) chemically crosslinked microspheres, CCMS, and (*b*) non-crosslinked microspheres, CCMS-CL

to non-dispersed microsphere aggregates. In the CCMS-CL sample, the volume-weighted median diameter is 105 μm. The results from the particle size analysis confirm the qualitative observations from FE-SEM that the CCMS-CL particles are larger on average than the CCMS ones. When epichlorohydrin was applied in the premixing of cellulose and chitosan solutions, a polymer network induced by crosslinked hydroxyl groups among cellulose and chitosan was established (Duan et al. 2015b). Since the crosslinked polymers were not as free or flexible as in the case of CCMS, where only physical interactions were present, larger spheres were preferably formed.

Conclusions

In this work we demonstrate the possibility of preparing cellulose–chitosan composite particles via different types of dissolution-regeneration procedures. By varying the conditions, particles of different sizes, of different morphologies and with different distributions of the two polysaccharides can be prepared. Specifically, novel cellulose–chitosan nano-composite particles were prepared by co-regeneration via dripping cellulose solutions in LiOH/urea into chitosan solution in acetic acid, or by mixing solutions of the two individual polymers in cold alkali/urea, followed by emulsification and co-regeneration with or without crosslinking agent. The results from XPS, FT-IR and elemental analysis signified that the bio-composite particles had different surface and bulk compositions. By comparing the nitrogen contents determined from XPS and elemental analysis, it was revealed that when mixing cellulose and chitosan solutions followed by emulsification, chitosan was evenly distributed from surface to core. The dripping method, on the other hand, mainly gave chitosan incorporated into the outermost surface layer of the particles. This implies that the distribution of chitosan in the composites can be easily tuned by the choice of preparation method. From FE-SEM and volume-average size distributions, it was found that the size of the particles can be controlled by the choice of preparation method. Thus our studies covered particle sizes from a few tenths of μm to a few mm. Furthermore, it was illustrated that the addition of a cross-linking agent affects porosity and can be used to vary particle morphology. In summary, it appears that this novel approach opens up opportunities to fabricate not only cellulose–chitosan composite particles with wide range of sizes and internal structures, but also nanocomposite materials in other forms; in turn this suggests a range of possible applications where cellulose's inherent strength is combined with chitosan's antibacterial properties.

Compliance with ethical standards

Conflict of interest The authors declare no competing financial interest.

References

Belgacem MN, Czeremuszkin G, Sapieha S, Gandini A (1995) Surface characterization of cellulose fibres by XPS and inverse gas chromatography. Cellulose 2:145–157

Bodvik R et al (2010) Aggregation and network formation of aqueous methylcellulose and hydroxypropylmethylcellulose solutions. Colloid Surf A 354:162–171

Bof MJ, Bordagaray VC, Locaso DE, García MA (2015) Chitosan molecular weight effect on starch-composite film properties. Food Hydrocolloids 51:281–294

Burkatovskaya M, Tegos GP, Swietlik E, Demidova TN, Castano AP, Hamblin MR (2006) Use of chitosan bandage to prevent fatal infections developing from highly contaminated wounds in mice. Biomaterials 27:4157–4164

Cai J et al (2008) Dynamic self-assembly induced rapid dissolution of cellulose at low temperatures. Macromolecules 41:9345–9351

Cao Z et al (2016) A facile and green strategy for the preparation of porous chitosan-coated cellulose composite membranes for potential applications as wound dressing. Cellulose 23:1349–1361

Chang C, Duan B, Cai J, Zhang L (2010) Superabsorbent hydrogels based on cellulose for smart swelling and controllable delivery. Eur Poly J 46:92–100

Cheng M, Deng J, Yang F, Gong Y, Zhao N, Zhang X (2003) Study on physical properties and nerve cell affinity of composite films from chitosan and gelatin solutions. Biomaterials 24:2871–2880

Chundawat SPS et al (2011) Restructuring the crystalline cellulose hydrogen bond network enhances its depolymerization rate. J Am Chem Soc 133:11163–11174

Duan B et al (2015a) Highly biocompatible nanofibrous microspheres self-assembled from chitin in NaOH/Urea aqueous solution as cell carriers. Angew Chem Int Ed 54:5152–5156

Duan J, Liang X, Cao Y, Wang S, Zhang L (2015b) High strength chitosan hydrogels with biocompatibility via new avenue based on constructing nanofibrous architecture. Macromolecules 48:2706–2714

Edgar CD, Gray DG (2003) Smooth model cellulose I surfaces from nanocrystal suspensions. Cellulose 10:299–306

Fang Y, Duan B, Lu A, Liu M, Liu H, Xu X, Zhang L (2015) Intermolecular interaction and the extended wormlike chain conformation of chitin in NaOH/urea aqueous solution. Biomacromolecules 16:1410–1417

Freire MG, Teles ARR, Ferreira RAS, Carlos LD, Lopes-da-Silva JA, Coutinho JAP (2011) Electrospun nanosized cellulose fibers using ionic liquids at room temperature. Green Chem 13:3173–3180

Glasser W et al (2012) About the structure of cellulose: debating the Lindman hypothesis. Cellulose 19:589–598

Hao X et al (2015) Self-assembled nanostructured cellulose prepared by a dissolution and regeneration process using phosphoric acid as a solvent. Carbohyd Polym 123:297–304

Hasegawa M, Isogai A, Onabe F, Usuda M, Atalla RH (1992) Characterization of cellulose–chitosan blend films. J Appl Polym Sci 45:1873–1879

Huber T, Müssig J, Curnow O, Pang S, Bickerton S, Staiger MP (2011) A critical review of all-cellulose composites. J Mater Sci 47:1171–1186

Isogai A, Atalla RH (1998) Dissolution of cellulose in aqueous NaOH solutions. Cellulose 5:309–319

Jain D, Banerjee R (2008) Comparison of ciprofloxacin hydrochloride-loaded protein, lipid, and chitosan nanoparticles for drug delivery. J Biomed Mater Res, Part B 86B:105–112

Kamide K, Okajima K, Kowsaka K (1992) Dissolution of natural cellulose into aqueous alkali solution: role of supermolecular structure of cellulose. Polym J 24:71–86

Kingkaew J, Kirdponpattara S, Sanchavanakit N, Pavasant P, Phisalaphong M (2014) Effect of molecular weight of chitosan on antimicrobial properties and tissue compatibility of chitosan-impregnated bacterial cellulose films. Biotechnol Bioprocess Eng 19:534–544

Kiyozumi T et al (2006) Medium (DMEM/F12)-containing chitosan hydrogel as adhesive and dressing in autologous skin grafts and accelerator in the healing process. J Biomed Mater Res, Part B 79B:129–136

Klemm D, Philipp B, Heinze T, Heinze U, Wagenknecht W (2004) Comprehensive cellulose chemistry. Wiley-VCH, Weinheim, pp 1–7

Liebert T (2010) Cellulose solvents? Remarkable history, bright future. In: Cellulose solvents: for analysis, shaping and chemical modification, vol 1033. ACS Symposium Series, vol 1033. American Chemical Society, pp 3–54

Lindman B, Karlström G, Stigsson L (2010) On the mechanism of dissolution of cellulose. J Mol Liq 156:76–81

Medronho B, Lindman B (2014) Competing forces during cellulose dissolution: from solvents to mechanisms. Curr Opin Colloid Interface 19:32–40

Medronho B, Lindman B (2015) Brief overview on cellulose dissolution/regeneration interactions and mechanisms. Adv Colloid Interface 222:502–508

Medronho B, Romano A, Miguel M, Stigsson L, Lindman B (2012) Rationalizing cellulose (in)solubility: reviewing basic physicochemical aspects and role of hydrophobic interactions. Cellulose 19:581–587

Medronho B, Duarte H, Alves L, Antunes F, Romano A, Lindman B (2015) Probing cellulose amphiphilicity. Nord Pulp Pap Res J 30:58–66

Miyamoto I, Inamoto M, Matsui T, Saito M, Okajima K (1995) Studies on structure of cuprammonium cellulose I. A circular dichroism study on the dissolved state of cellulose in cuprammonium solution. Polym J 27:1113–1122

Nishino T, Takano K, Nakamae K (1995) Elastic modulus of the crystalline regions of cellulose polymorphs. J Polym Sci Polym Phys 33:1647–1651

Nishio Y (1994) Hyperfine composites of cellulose with sythetic polymers. In: Gilbert RD (ed) Cellulosic polymers, blends and composites. Hanser Publishers, Munich, p 157

Peter MG (1995) Applications and environmental aspects of chitin and chitosan. J Macromol Sci A 32:629–640

Philipp B (1993) Organic solvents for cellulose as a biodegradable polymer and their applicability for cellulose spinning and derivatization. J Macromol Sci A 30:703–714

Pillai CKS, Paul W, Sharma CP (2009) Chitin and chitosan polymers: chemistry, solubility and fiber formation. Prog Polym Sci 34:641–678

Qiu X, Hu S (2013) Smart" Materials based on cellulose: a review of the preparations, properties, and applications. Materials 6:738–781

Rosenau T, Potthast A, Adorjan I, Hofinger A, Sixta H, Firgo H, Kosma P (2002) Cellulose solutions in N-methylmorpholine-N-oxide (NMMO)—degradation processes and stabilizers. Cellulose 9:283–291

Saalwächter K, Burchard W, Klüfers P, Kettenbach G, Mayer P, Klemm D, Dugarmaa S (2000) Cellulose solutions in water containing metal complexes. Macromolecules 33:4094–4107

Shepherd R, Reader S, Falshaw A (1997) Chitosan functional properties. Glycoconj J 14:535–542

Trygg J (2015) Functional cellulose microspheres for pharmaceutical applications. Åbo akademi University, Turku

Wang Q, Cai J, Chen K, Liu X, Zhang L (2016) Construction of fluorescent cellulose biobased plastics and their potential application in anti-counterfeiting banknotes. Macromol Mater Eng 301:377–382

Wu Y et al (2016) Green and biodegradable composite films with novel antimicrobial performance based on cellulose. Food Chem Part A 197:250–256

Xiang Q, Yu J, Wang W, Jaroniec M (2011) Nitrogen self-doped nanosized TiO_2 sheets with exposed {001} facets for

enhanced visible-light photocatalytic activity. Chem Commun 47:6906–6908

Yamashiki T, Kamide K, Okajima K (1990) New cellulose fiber from aqueous alkali cellulose solution. In: Kennedy JF, Phillips GO, Williams PA (eds) Cellulose sources and exploitation: industrial utilization, biotechnology and physico-chemical properties. Ellis Horwood, Chichester, p 197

Yang Y et al (2012) One-step synthesis of amino-functionalized fluorescent carbon nanoparticles by hydrothermal carbonization of chitosan. Chem Commun 48:380–382

Zhang L, Ruan D, Gao S (2002) Dissolution and regeneration of cellulose in NaOH/thiourea aqueous solution. J Polym Sci Polym Phys 40:1521–1529

Zhang Y, Xue C, Xue Y, Gao R, Zhang X (2005) Determination of the degree of deacetylation of chitin and chitosan by X-ray powder diffraction. Carbohyd Res 340:1914–1917

Zhang D-Y, Duan M-H, Yao X-H, Fu Y-J, Zu Y-G (2016) Preparation of a novel cellulose-based immobilized heteropoly acid system and its application on the biodiesel production. Fuel 172:293–300

Zhou J, Zhang L (2000) Solubility of cellulose in NaOH/urea aqueous solution. Polym J 32:866–870